

BaF₂:Y and ZnO:Ga crystal scintillators for GHz hard X-ray imagingChen Hu^a, Liyuan Zhang^a, Ren-Yuan Zhu^{a,*}, Aiping Chen^b, Zhehui Wang^b, Lei Ying^c, Zongfu Yu^c^a California Institute of Technology, 1200 E California Blvd, Pasadena, CA 91125, USA^b Los Alamos National Laboratory, Los Alamos, NM 87545, USA^c University of Wisconsin, Madison, WI 53706, USA

ARTICLE INFO

Keywords:

Ultrafast crystal
Ultrafast photodetector
Hard X-ray imaging
Microchannel plate photomultiplier
Rise time
Decay time
FWHM pulse width

ABSTRACT

Gigahertz (GHz) hard X-ray imaging for the proposed MaRIE project presents an unprecedented challenge for the front imager in both speed and radiation hardness. We proposed two ultrafast inorganic-scintillator-based front imager concepts: a total absorption one and a multilayer one, and investigated optical and scintillation properties for a set of inorganic scintillators at the Caltech HEP crystal laboratory. The results show that yttrium doped barium fluoride crystals and gallium doped ZnO nano-particle-based films are promising for these two concepts, respectively. In this paper, we report their optical and scintillation property as well recent progresses on slow component suppressing in barium fluoride crystals by yttrium doping, and its radiation hardness.

Contents

1. Introduction	1
2. Samples and measurements	2
3. Experimental results.....	2
3.1. Optical property and scintillation performance.....	2
3.2. Radiation hardness of BaF ₂ crystals	4
4. Summary	6
Acknowledgments	7
References.....	7

1. Introduction

Aiming at studying the dynamics of material evolution related to the nuclear Big Bang, the matter–radiation interaction in extreme (MaRIE) experimental facility was proposed for high-energy X-ray free electron lasers at Los Alamos [1], where gigahertz hard X-ray (>20 keV) imaging is required [2]. Two types of high-energy X-ray imagers were on demand [3]. While the Type-I imager requires a 50% efficiency for 30 keV X-rays, a frame-rate of 500 MHz and a 300 μm pixel size, the Type-II imager requires 80% efficiency for 42 keV to 126 keV X-rays, a frame-rate of 3 GHz and a less than 300 μm pitch [3]. Significant gaps exist between the state-of-the-art high-speed X-ray imaging of both direct and in-direct technologies and the MaRIE requirements. The ultrafast frame rates require ultrafast sensors to capture and store the dense spatial and temporal signals. The hard X-rays require sufficient thick detector for the best efficiency and dynamic range. To mitigate pileup

effect for such high frame rates, it is important to have a temporal response of less than 2 ns and 300 ps respectively for the Type I and II imagers. The development of sensors with ultrafast temporal response is thus crucial.

We propose two ultrafast-inorganic-scintillator-based detector concepts for GHz hard X-ray imaging: a total absorption concept and a multilayer concept. Fig. 1 is a schematic showing the total absorption concept consisting of a pixelated ultrafast crystal screen coupled to an ultrafast pixelated ultrafast photodetector followed by an ultrafast readout electronics [3]. This concept is inspired by the total absorption crystal calorimetry in high physics experiments. The advantage of this concept is its high absorption efficiency for hard X-rays up to 120 keV. With a 5 mm thick crystal screen almost 100% X-rays are absorbed in the crystal screen, providing the maximum dynamic range offered by X-ray pulses. A limiting factor for this concept is its spatial resolution which is limited by the pixel size, or pitch. While typical pitch provided

* Corresponding author.

E-mail address: zhu@hep.caltech.edu (R.-Y. Zhu).

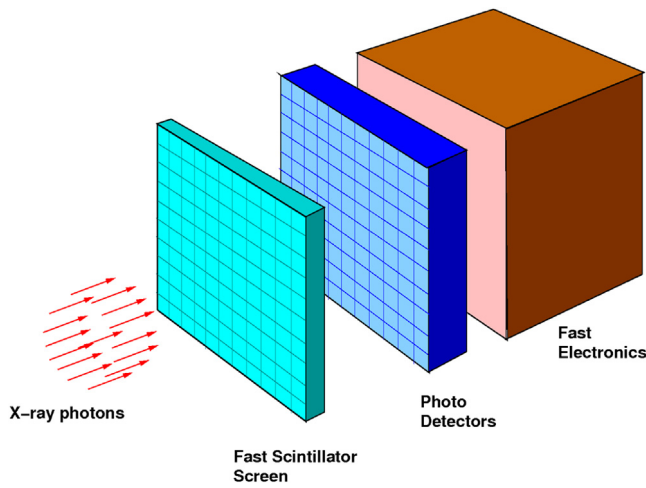


Fig. 1. A pixelated ultrafast crystal-based total absorption front imager concept.

by mechanical dicing technology is 300 μm , the state-of-the-art laser dicing technology may provide a fine pitch down to 25 μm . Fig. 2 shows the multilayer detector concept, where each layer consists of an ultrafast scintillator thin film coated with high quantum efficiency (QE) photocathode layer, a magnetic field perpendicular to the X-ray direction guides the photoelectrons to amplification and storage [4]. The advantage of this concept is high spatial resolution anti-proportional to the crystal film thickness. The disadvantage of this concept is the low X-ray absorption efficiency limited by the crystal layer thickness, and the degraded spatial resolution along the X-ray path due to dead material between crystal films.

In our previous investigation, we studied optical and scintillation properties for a set of fast inorganic scintillators at the Caltech HEP crystal lab, including four groups of inorganic scintillator according to their scintillation mechanism [5]. The first group is the direct-gap semiconductor crystals, such as gallium-doped ZnO (ZnO:Ga). The second group is the core-valence luminescence crystals, such as barium fluoride (BaF_2) and yttrium-doped barium fluoride ($\text{BaF}_2:\text{Y}$). The third group is Yb^{3+} activated crystals featured with fast decay time and thermal quenching, such as $\text{YAlO}_3:\text{Yb}$ (YAP:Yb) and $\text{Y}_3\text{Al}_5\text{O}_{12}:\text{Yb}$ (YAG:Yb). The fourth group is Ce^{3+} activated bright and fast crystals, such as cerium doped lutetium yttrium oxyorthosilicate $\text{LYSO}:\text{Ce}$ ($\text{Lu}_{2(1-x)}\text{Y}_{2x}\text{SiO}_5:\text{Ce}$ or LYSO) and yttrium oxyorthosilicate ($\text{Y}_2\text{SiO}_5:\text{Ce}$ or YSO:Ce), YAlO_3 (YAP:Ce), $\text{Lu}_3\text{Al}_5\text{O}_{12}:\text{Ce}$ (LuAG:Ce), and $\text{LaBr}_3:\text{Ce}$. Based on this investigation, we propose yttrium doped barium fluoride single crystal ($\text{BaF}_2:\text{Y}$) and gallium doped zinc oxide (ZnO:Ga) nano particle based films for the two detector concepts, respectively. In this paper, we report their optical and scintillation properties, recent progresses on slow component suppressing in barium fluoride by yttrium doping and its radiation hardness, as well as our plan for future R&D.

2. Samples and measurements

Table 1 lists BaF_2 , $\text{BaF}_2:\text{Y}$ and ZnO:Ga samples used in this investigation, including crystal types, vendors, sample dimensions and experimental measurements performed. Fig. 3 shows photos of one BaF_2 , one $\text{BaF}_2:\text{Y}$ and two ZnO:Ga samples. Transmittance was measured by using a PerkinElmer Lambda 950 spectrophotometer with 0.15% precision. Photoluminescence (PL) was measured by using an Edinburgh Instruments FLS 920 fluorescence spectrometer. For the X-ray excited luminescence (XEL) measurements, samples were placed in the sample compartment of a HITACHI F-4500 spectrophotometer. X-rays generated by an Amptek Eclipse-III X-ray tube were used to excite the sample. Light output (LO) of BaF_2 samples was measured by using a Hamamatsu R2059 PMT and 0.511 MeV γ -rays from a ^{22}Na

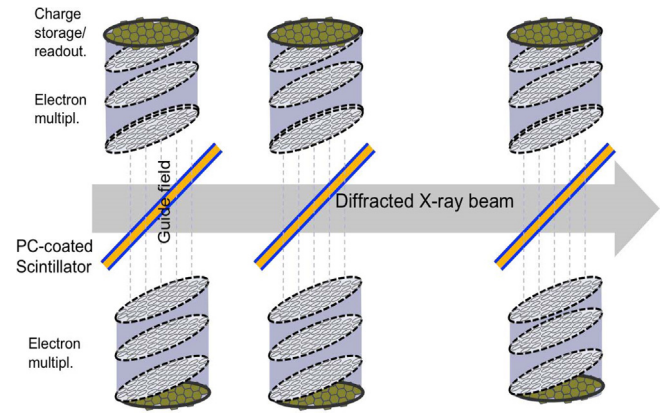


Fig. 2. An ultrafast crystal film-based multi-layer front imager concept.

source with a coincidence trigger to mitigate residual phosphorescence in the samples. Because of its low LO due to self-absorption, LO of ZnO:Ga samples was measured by using a Hamamatsu R2059 PMT for 5.486 MeV α -particles from an ^{241}Am source.

In all these LO measurements, the samples were wrapped with two layers of Tyvek paper, and the PMTs were coupled to the sample via a thin layer of Down-Corning 200 optical fluid. The systematic uncertainty of the LO measurement is about 1% [6]. The scintillation pulses from R2059 were integrated and analyzed by a home-made LeCroy QVT based MCA system. Scintillation pulse shape and decay time were measured by using a Hamamatsu R2059 PMT and an Agilent 9254 digital scope with a temporal response time of 1.3 and 0.14 ns, respectively. A ^{22}Na source was used as the excitation source, of which two 511 keV gammas excited the sample and a small BaF_2 crystal providing a coincidence trigger. Note, the slow response of the R2059 PMT limited our ability to measure sub-nanoseconds decay time. Temporal response of these samples was also measured by MCP-PMTs for picosecond X-ray pulses at Advanced Photon Source [7]. Gamma irradiations were carried out by using ^{137}Cs and ^{60}Co sources at Caltech and the Jet Propulsion Laboratory, respectively. Proton and neutron irradiations were carried out by using 800 MeV protons and fast neutrons at the Weapons Neutron Research facility of Los Alamos Neutron Science Center (LANSCE). Sample's LO, transmittance and decay kinetics were measured before and after irradiations at Caltech HEP crystal lab.

3. Experimental results

3.1. Optical property and scintillation performance

Fig. 4 shows the transmittance (black lines) and the PL spectrum (blue dashes) for the ZnO:Ga crystal sample of $22 \times 22 \times 0.3 \text{ mm}^3$. Also shown in the figure is theoretical limit (black dots) of transmittance calculated according to its refractive index. A large fraction of the emission peaked at 380 nm is below the transmittance edge at 400 nm, indicating a serious self-absorption. In addition, the discrepancy between the measured transmittance and the theoretical limit implies that the quality of the ZnO:Ga crystal sample may be further improved. We also noticed that the 2 mm thick ZnO:Ga sample shows a similar emission and more severe self-absorption as compared to the 0.3 mm sample.

Fig. 5 shows the pulse height spectrum of the $22 \times 22 \times 0.3 \text{ mm}^3$ ZnO:Ga sample excited by 5-MeV α -particles. A LO of 296 p.e./MeV was observed. Because of their very short absorption length in the crystal the 5-MeV α -particles excited only a thin-layer at crystal's surface. Most scintillation photons generated by the α -particles propagated across the entire thickness before reaching the photodetector. Because of the self-absorption, the LO of $33 \times 30 \times 2 \text{ mm}^3$ ZnO:Ga sample was measured to be 76 p.e./MeV, much lower than that from the

Table 1
BaF₂, BaF₂:Y and ZnO:Ga crystal samples investigated in this work.

Samples	Vendors	Dimensions (mm ³)	Quantity	Measurement and experiments
BaF ₂	SIC	50 × 50 × 5	1	PL, T, LO and Decay
BaF ₂ :Y(0%–7%)	BGRI	∅18 × 21	9	XEL
BaF ₂	BGRI	10 × 10 × 5	4	LO and Decay
BaF ₂ :Y	BGRI	10 × 10 × 5	4	LO and Decay
BaF ₂	BGRI	30 × 30 × 200	1	γ induced damage
BaF ₂	SIC	25 × 25 × 250	1	γ induced damage
BaF ₂	Incrom	30 × 30 × 200	1	γ induced damage
BaF ₂	SIC	25 × 25 × 5	6	Proton induced damage
BaF ₂	SIC	15 × 15 × 5	6	Neutron induced damage
ZnO:Ga	FJIRSM	33 × 30 × 2	1	PL, T, LO and Decay
ZnO:Ga	FJIRSM	22 × 22 × 0.3	1	PL, T, LO and Decay

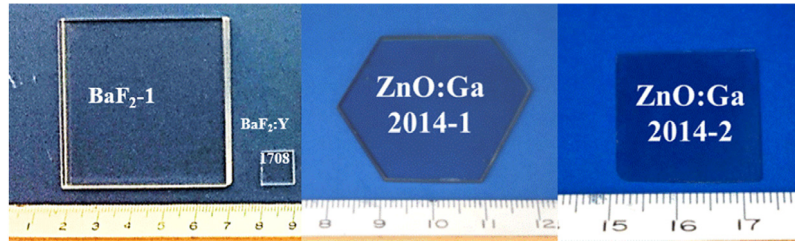


Fig. 3. A photo showing one BaF₂, one BaF₂:Y and two ZnO:Ga samples.

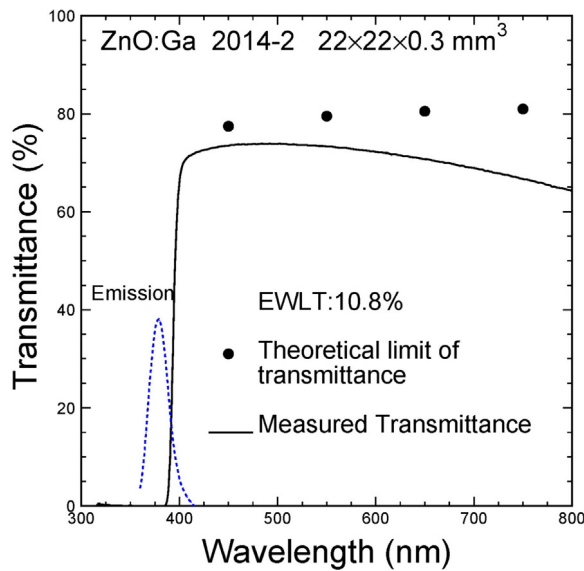


Fig. 4. The transmittance and PL spectrum of the ZnO:Ga crystal sample of $22 \times 22 \times 0.3 \text{ mm}^3$.

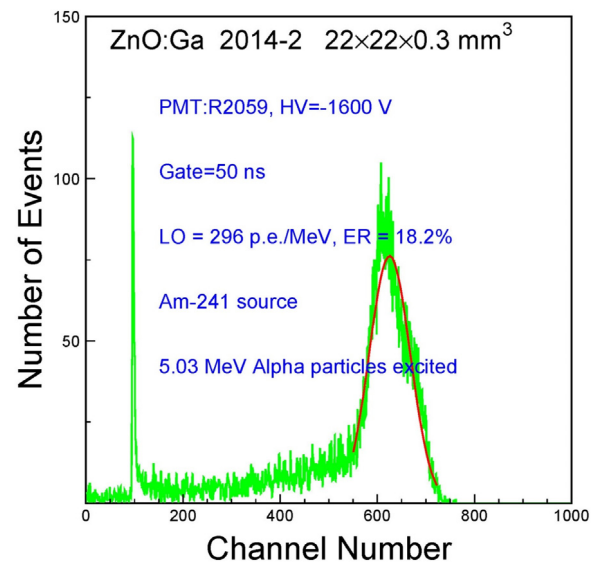


Fig. 5. The pulse height spectrum for the ZnO:Ga sample of $22 \times 22 \times 0.3 \text{ mm}^3$ excited by 5.03 MeV α -particles.

0.3 mm sample. Fig. 6 shows the pulse shape obtained from the 0.3 mm thick ZnO:Ga sample excited by 0.511-MeV γ -ray from a ²²Na source, which is basically consistent with that obtained from the 2 mm thick ZnO:Ga. The observed decay time is a few nanoseconds, which is longer than the 0.5-ns decay time observed from the ZnO:Ga nanoparticles embedded in polystyrene [8–10], partly due to the temporal response time of the R2059 PMT used in this measurement.

BaF₂ is a core valence scintillator in which the energy gap between the valence band and the uppermost core band is less than the fundamental bandgap. A photon is emitted when an electron in the valence band fills an ionization hole in the top core band, which is so-called cross-luminescence with a decay time of less than 1 ns [11–13]. In addition to this sub-nanosecond fast component peaked at 220 nm, BaF₂ has also a slow component peaked around 300 nm with a decay time of about 600 ns. Fig. 7 shows the transmittance and emission

spectrum for the BaF₂ crystal sample of $50 \times 50 \times 5 \text{ mm}^3$. Also shown in this plot are the numerical values of the emission weighted longitudinal transmittance (EWLT) for the fast (220 nm) and the slow (300 nm) components. We notice that BaF₂ has a good transmittance without self-absorption, so may be used for the total absorption detector concept. Fig. 8 shows its pulse height spectrum measured by an R2059 PMT with an integration time of 50 ns for the 0.511 MeV γ -rays from a ²²Na source. While the LO is 209 p.e./MeV, the full-width at half-maximum (FWHM) resolution is 55%. Fig. 9 shows its LO as a function of the integration time up to 4 μ s and corresponding exponential fit, where the amplitudes of the fast component (A_0) and the slow component (A_1) are extracted. It is clear that the slow component has an intensity of about a factor of eight of the fast component. Since the slow scintillation component causes pileup, so needs to be suppressed for applications where a high counting rate is expected.

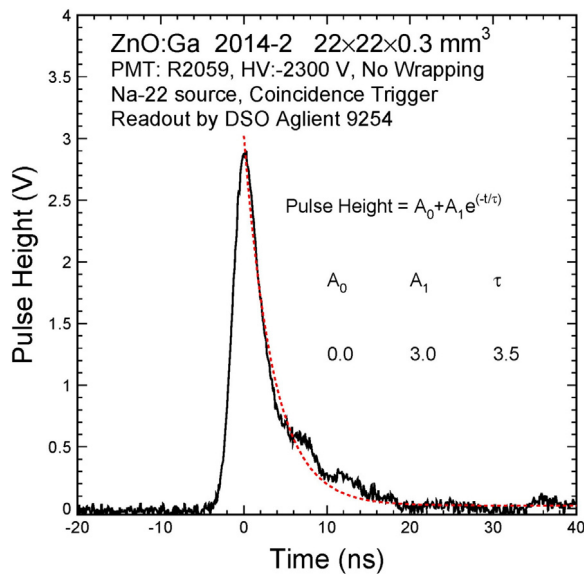


Fig. 6. The pulse shape for the ZnO:Ga sample of $22 \times 22 \times 0.3 \text{ mm}^3$ excited by ^{22}Na γ -rays.

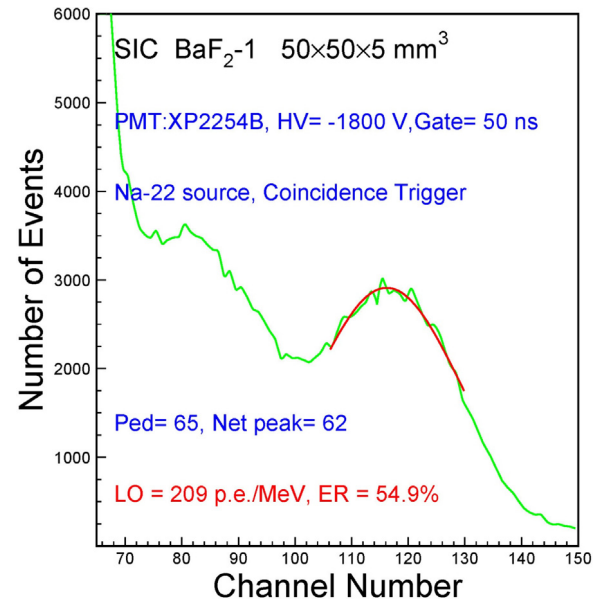


Fig. 8. A pulse height spectrum for the BaF_2 crystal sample of $50 \times 50 \times 5 \text{ mm}^3$ excited by ^{22}Na γ -rays.

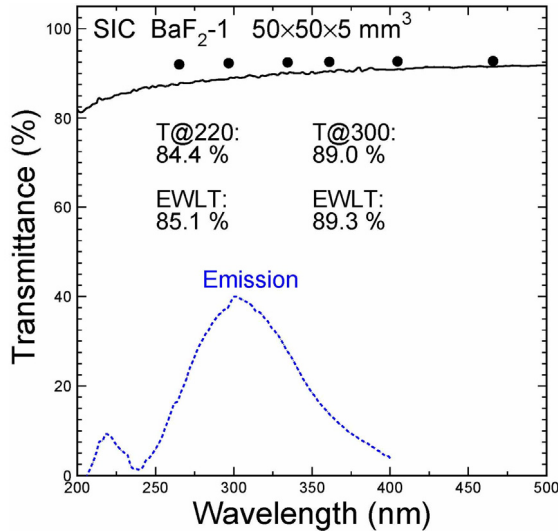


Fig. 7. The transmittance and PL spectrum for the BaF_2 crystal sample of $50 \times 50 \times 5 \text{ mm}^3$.

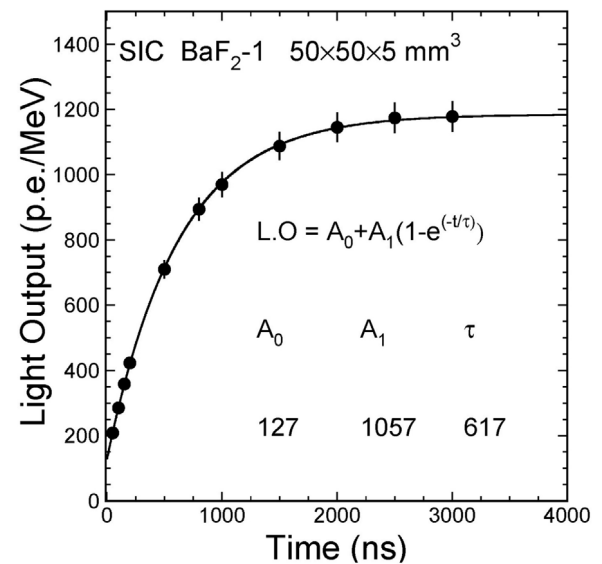


Fig. 9. The LO of the BaF_2 crystal sample of $50 \times 50 \times 5 \text{ mm}^3$ is shown as a function of the integration time.

Two approaches have been pursued to mitigate the slow component: (1) selective doping with rare earth in BaF_2 and (2) selective readout with solar blind photodetector. A yttrium doping experiment was carried out at Beijing Glass Research Institute (BGRI) [14]. Fig. 10 shows X-ray excited emission spectra for five yttrium doped BaF_2 crystal samples selected from a set of a total of nine samples of $\Phi 18 \times 21 \text{ mm}^3$ from BGRI with the yttrium doping level from 0 mol% to 7 mol%. While all samples have similar values of the fast component, it was found that the sample with 5 mol% yttrium doping showed the smallest slow component. Figs. 11 and 12 show the LO as a function of the integration time and the corresponding exponential fit for four each of BaF_2 and 5 mol% doped $\text{BaF}_2:\text{Y}$ crystal samples of $10 \times 10 \times 5 \text{ mm}^3$, respectively. The average fast/slow ratio (A_0/A_1) is improved from 1/5 to 3/1, indicating that yttrium doping is effective for the slow component suppression in BaF_2 crystals.

3.2. Radiation hardness of BaF_2 crystals

We measured radiation hardness against γ -rays for three 20 cm long BaF_2 samples from different vendors [15]. It was found that the γ -ray-induced radiation damage is not dose rate dependent. Fig. 13 shows normalized emission weighted longitudinal transmittance (EWLT, top) and LO (bottom) as a function of integrated dose up to 120 Mrad for the fast component (220 nm) for three long crystals from different vendors. While the sample SIC2012 was grown by SICCAS in 2012, the samples BGRI 2015 and Incrom 2015 were grown in 2015 by BGRI and Incrom respectively. The average EWLT and LO values after 120 Mrad were found to be 40% and 45% respectively for the fast and the slow scintillation component respectively in these samples from three different vendors, indicating that long crystals with good radiation hardness against ionization dose up to 120 Mrad are commercially available. Fig. 14 shows the average values of the radiation induced

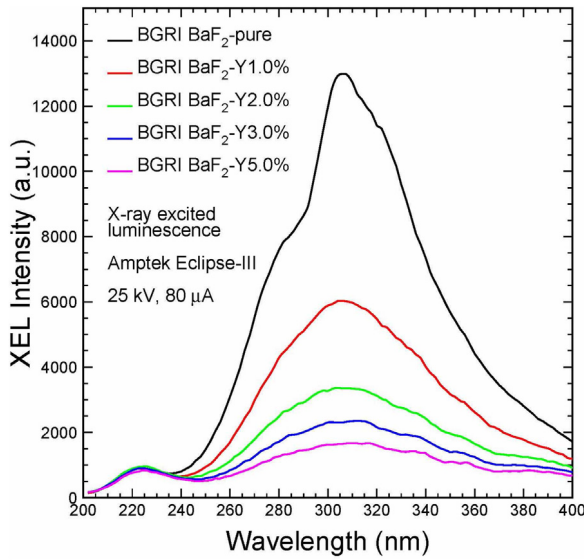


Fig. 10. The XEL spectra for BaF₂ samples of ϕ 18 × 20 mm³ doped with yttrium (0, 1.0, 2.0, 3.0 and 5.0 mol%).

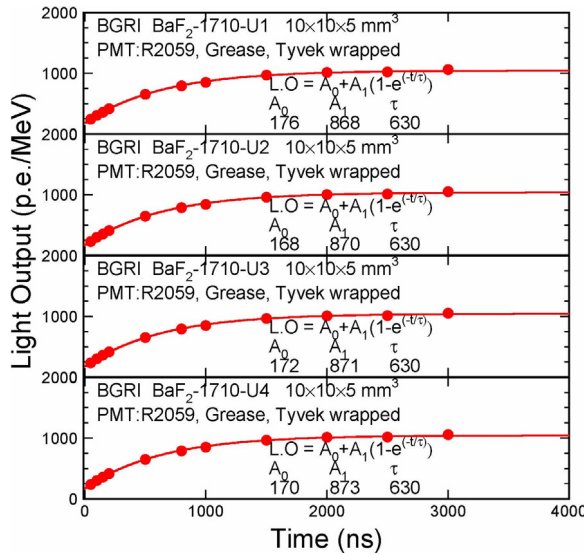


Fig. 11. The LO of four undoped BaF₂ samples of 10 × 10 × 5 mm³ are shown as a function of the integration time.

absorption coefficient (RIAC) at the emission peak as a function of the integrated dose for various crystal samples. BaF₂ is much better than CeF₃, PWO and CsI, although slightly worse than LYSO and BGO.

We also measured radiation hardness of BaF₂ crystal against 800 MeV protons at LANSCE [16]. A total of 18 crystal samples of 5 mm thick BaF₂ and PWO and 3 mm thick LYSO were irradiated in 2016 in three groups with a proton fluence of 0.27, 1.6, and 9.7 × 10¹⁴ p/cm², respectively. Fig. 15 summarizes the EWRIAC values as a function of the proton fluence, calculated by using the LT spectra data measured at Caltech before and 181 days after the irradiations. They are 7, 18, and 71 m⁻¹ respectively for LYSO, BaF₂, and PWO after a proton fluence of 9.7 × 10¹⁴ p/cm², indicating excellent radiation hardness of LYSO and BaF₂ crystals against charged hadrons. Fig. 16 summarizes the normalized LO as a function of the proton fluence for BaF₂, LYSO, and PWO, measured at Caltech before and 181 days after proton irradiation. The LO losses after a proton fluence of 9.7 × 10¹⁴ p/cm² are 10% and 13% respectively for the LYSO and BaF₂ samples, confirming their excellent radiation hardness against charged hadrons. The LO of PWO

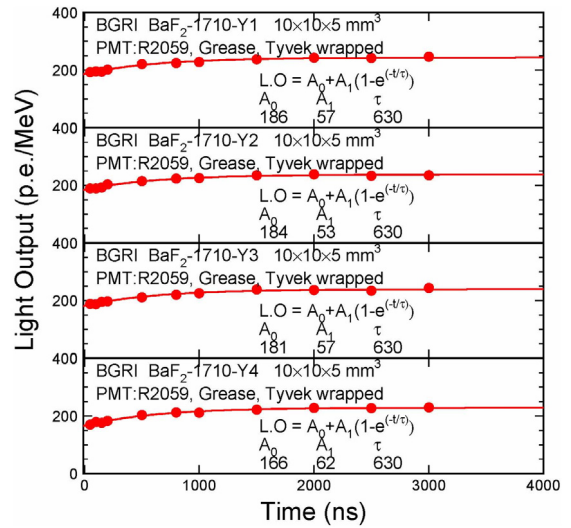


Fig. 12. The LO of four BaF₂:Y samples of 10 × 10 × 5 mm³ are shown as a function of the integration time.

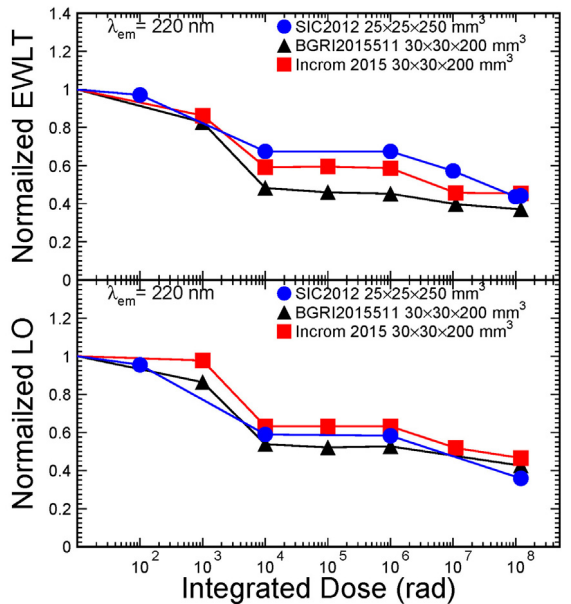


Fig. 13. The normalized EWL (top) and LO (bottom) of the fast component are shown as a function of the integrated dose for crystals from three vendors.

samples after a proton fluence of 9.7 × 10¹⁴ p/cm² is too low to be experimentally determined.

Similarly, a total of 36 of 5 mm thick LYSO, BaF₂ and PWO samples in three groups were irradiated at the East Port of LANSCE in 2016 to reach a fast neutron (>1 MeV) fluence of 7.4, 16, and 36 × 10¹⁴ n/cm² respectively [17]. Half samples in each group were shielded with 5 mm Pb to understand the effect of accompanying γ -rays at the East port. Fig. 17 shows transmittance spectra before and after irradiation for one each of LYSO (top), BaF₂ (middle) and PWO (bottom) samples in the group 3. Also shown in the figure are the corresponding theoretical limit of transmittance (black dots) for each crystal calculated by using crystal's refractive index assuming multiple bounces and no internal absorption. Excellent optical quality was observed in these samples before irradiation. Also listed in the figure are the numerical values of EWL, which are 71.4%, 74.4%, and 39.6% respectively for LYSO, BaF₂, and PWO after a fast neutron fluence of 3.6 × 10¹⁵/cm², indicating a much better radiation resistance of LYSO and BaF₂ than PWO. Fig. 18 shows

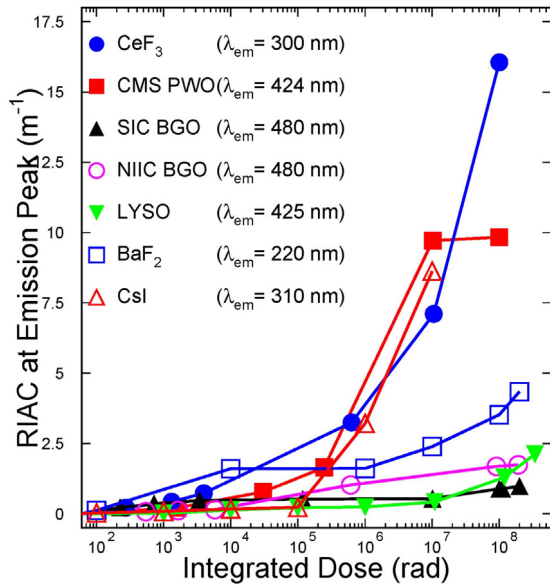


Fig. 14. The RIAC values at the emission peak are shown as a function of integrated dose for various crystals.

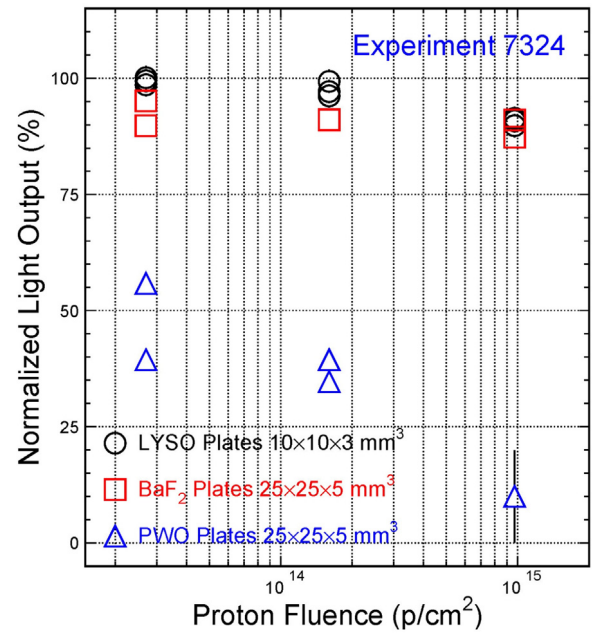


Fig. 16. The normalized LO is shown as a function of the proton fluence for BaF₂, LYSO, and PWO crystals.

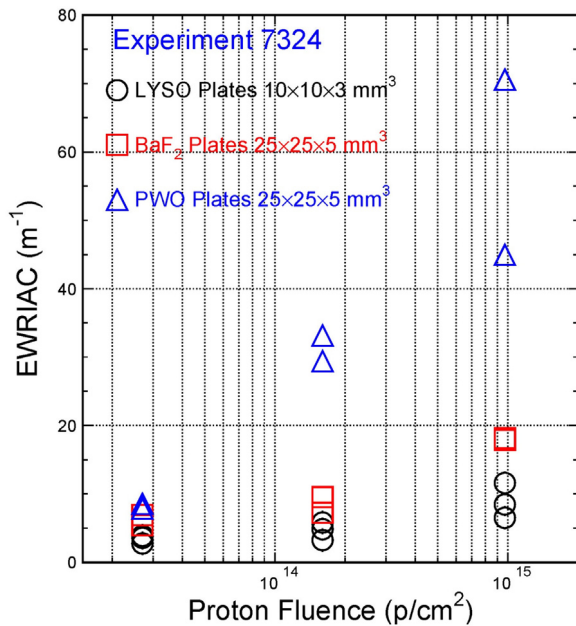


Fig. 15. The EWRIAC values are shown as a function of the proton fluence for BaF₂, LYSO, and PWO crystals.

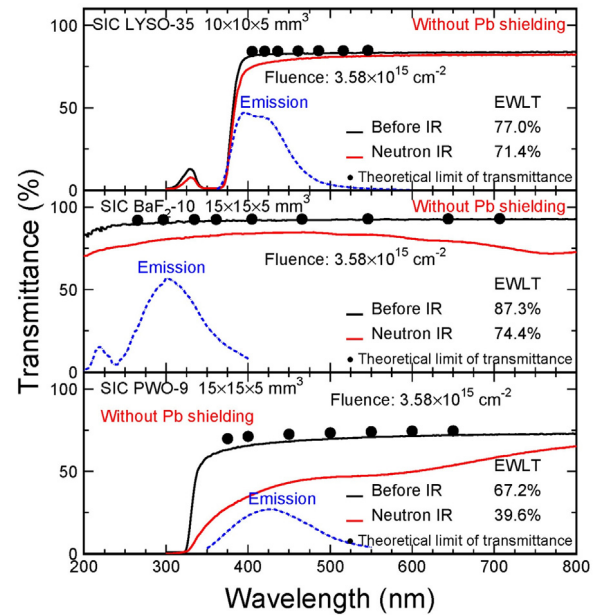


Fig. 17. The transmittance spectra before and after irradiation are shown for one sample each of LYSO (top), BaF₂ (middle) and PWO (bottom) without Pb shielding.

the normalized LO as a function of the fast neutron fluence for LYSO, BaF₂ and PWO samples. Each LO value is the average of two samples irradiated with the same condition. The normalized LO values are 77% and 76% respectively for LYSO and BaF₂ crystals without Pb shielding, and 80% with Pb shielding. In both cases, the LO of PWO samples in the group 3 is too low to be measured in the lab after neutron (>1 MeV) fluence of 3.6×10^{15} n/cm². It is clear that LYSO and BaF₂ are much more radiation hard than PWO under neutron irradiations.

4. Summary

Because of their sub-nanosecond decay time and high absorption efficiency for hard X-rays, BaF₂:Y and ZnO:Ga crystal scintillators are identified as promising ultrafast inorganic scintillators for two front

imaging concepts for the hard X-rays from the proposed MaRIE free electron lasers. While BaF₂ is a mature crystal in both crystal growth and commercial availability, the main issue is its slow component around 300 nm with a decay time of about 600 ns. Our investigation revealed that yttrium doping is effective in suppressing the slow component while maintaining the ultrafast component. The averaged fast/slow ratio is improved from about 1:5 to 3:1, and is expected to be further improved by on-going R&D.

Radiation hardness of BaF₂ against γ -rays was measured for samples of 20 cm long by using Co-60 gamma source at Caltech and JPL up to an ionization dose of 120 Mrad. The degradation of their light output was saturated after 10 krad with remaining light output at about 45%

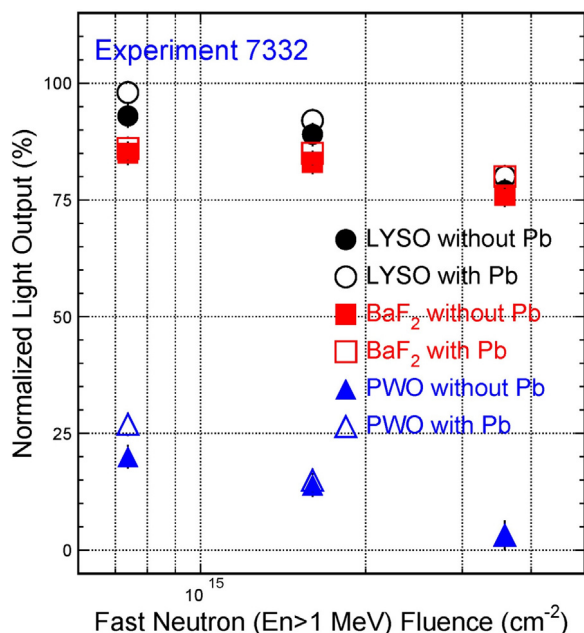


Fig. 18. The normalized LO is shown as a function of the fast neutron fluence for LYSO, BaF₂ and PWO samples.

after 120 Mrad. The proton and fast neutron irradiation experiments were carried out at LANSCE for 5 mm thick BaF₂ plates, irradiated by 800 MeV protons of up to 9.7×10^{14} p/cm² and fast neutrons (>1 MeV) of up to 3.6×10^{15} p/cm² respectively. The results confirmed its excellent radiation hardness with a light output loss of less than 25%.

While ZnO:Ga crystals show promising ultrafast scintillation, its main issue is self-absorption. This material thus may be used in the multi-layer front imager concept. Its radiation hardness, however, has not been measured. We plan to pursue both ZnO:Ga crystals and thin films, and test their radiation hardness.

Acknowledgments

This work is supported by the U.S. Department of Energy, Office of High Energy Physics, USA program under Award Number DE-SC0011925.

References

- [1] R.W. Garnett, M.S. Gulley, Matter-radiation interactions in extremes, in Proc. Linear Accelerator Conf. (LINA), 2010, 485–487.
- [2] Z. Wang, et al., Gigahertz (GHz) hard X-ray imaging using fast scintillators, Proc. SPIE, Hard X-ray, Gamma-Ray, Neutron Detector Phys. XV, 8852, 88521A, Sep. 2013.
- [3] Ultrafast and high-energy X-ray imaging technologies and applications, Los Alamos Nat. Lab. Santa Fe, NM, USA, Tech. Rep. LA-UR-17-22085, Aug. 2016. See imager concept by R.-Y. Zhu. Online Available: https://www.lanl.gov/science-innovation/science-facilities/marie/_assets/docs/workshops/ultrafast-high-energy-x-ray.pdf.
- [4] Z. Wang, et al., Thin scintillators for ultrafast hard X-ray imaging, Proc. SPIE, Photon Counting Appl. 9504, 95040N, 2015.
- [5] Chen Hu, et al., Ultrafast inorganic scintillators for Gigahertz Hard X-ray imaging, IEEE Trans. Nucl. Sci. 65 (8) (2018) 2097–2104.
- [6] X. Qu, et al., A study on yttrium doping in lead tungstate crystals, Nucl. Instrum. Methods Phys. Res. A 480 (2002) 470–487.
- [7] Chen Hu, et al., Ultrafast inorganic scintillator-based front imager for Gigahertz Hard X-ray imaging, Nucl. Instrum. Methods Phys. Res. A 940 (2019) 223–229.
- [8] S.E. Derenzo, M.J. Weber, M.K. Klintonberg, Temperature dependence of the fast, near-band-edge scintillation from CuI, HgI₂, PbI₂, ZnO:Ga and CdS:In, Nucl. Instrum. Methods Phys. Res. A 486 (2002) 214–219.
- [9] E. Ohshima, et al., Growth of the 2-in-size bulk ZnO single crystals by the hydrothermal method, J. Cryst. Growth 260 (1–2) (2004) 166–170.
- [10] H. Buresova, Preparation and luminescence properties of ZnO:Ga – polystyrene composite scintillator, OPTICS EXPRESS 24 (14) (2016) 15289.
- [11] A.P. Shpak, O.A. Glike, A.G. Dmitriev, P.A. Rodnyi, A.S. Voloshinovskii, S.M. Pidzyrailo, Radiative core-valence transitions in wide-gap crystals, J. Electron. Spectrosc. Relat. Phenom. 68 (1994) 335–338.
- [12] P.A. Rodnyi, Core-valence transitions in wide-gap ionic crystals, Sov. Phys. Solid-State 34 (7) (1992) 1053–1066.
- [13] M.J. Weber, Scintillation: mechanisms and new crystals, Nucl. Instrum. Methods Phys. Res. A 527 (1–2) (2004) 9–14.
- [14] R.-Y. Zhu, 'Applications of Very Fast Inorganic Crystal Scintillators in Future HEP Experiments', TIPP 2017, SPPHY 213, (2018) 70–75, http://dx.doi.org/10.1007/978-981-13-1316-5_13.
- [15] F. Yang, L. Zhang, R.-Y. Zhu, Gamma-ray induced radiation damage up to 340 Mrad in various scintillation crystals, IEEE Trans. Nucl. Sci. 63 (2) (2016) 612–619.
- [16] Chen Hu, et al., Proton-induced radiation damage in BaF₂, LYSO, and PWO crystal scintillators, IEEE Trans. Nucl. Sci. 65 (4) (2018) 1018–1024.
- [17] Chen Hu, et al., Neutron-induced radiation damage in BaF₂, LYSO/LFS and PWO Crystals, J. Phys.: Conf. Ser. 1162 (2019) 012020.